

Trafficking motifs as the basis for two-compartment signaling systems to form multiple stable states

Upinder S. Bhalla¹

¹National Centre for Biological Sciences, Tata Institute of Fundamental Research, Bellary Road, Bangalore 560065, India.

Supporting Material.

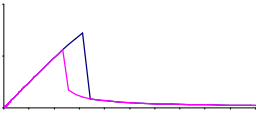
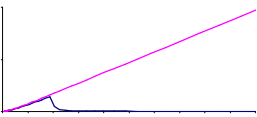
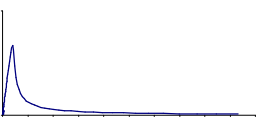
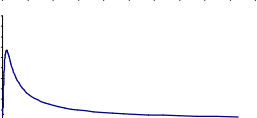
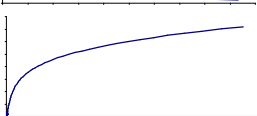
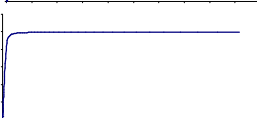
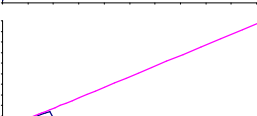
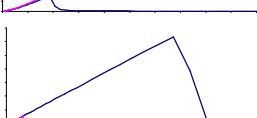
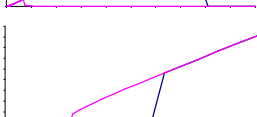
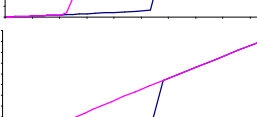
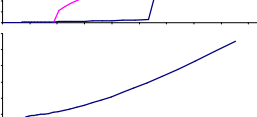
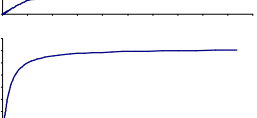
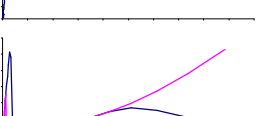
Contents:

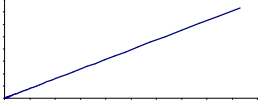

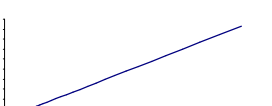
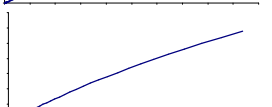
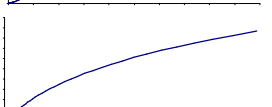
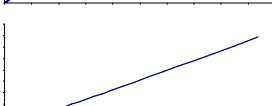
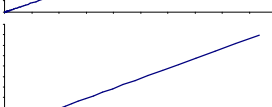
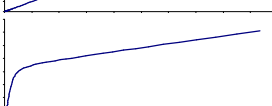
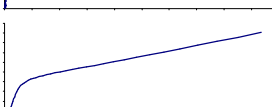
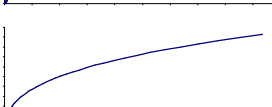
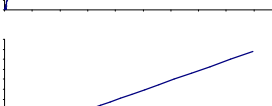
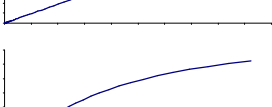
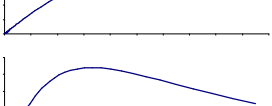
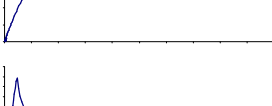
Supporting Table S1

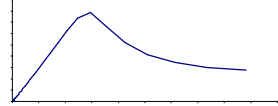
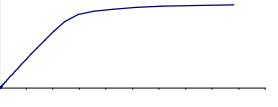
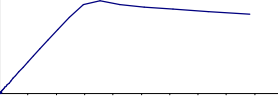
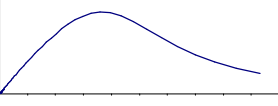
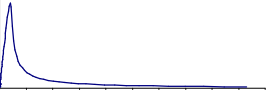
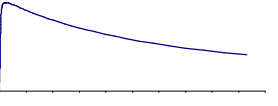
Supporting Table S2

Supporting Figure S1

Supporting Text S1 (Methods).

# Description	Citation	Shape		Model and plot name. If they differ, the plotname is in brackets.	Input molecule	Output molecule
1 Positive feedback, bistable	1, 2	bis		fb_bis	A/M	A/M*
2 dual phosphorylation, bistable	3	bis		Markevich	K	Kpp
3 Positive feedback, non-bistable	Adapted from 1	neg		fb_neg	A/M	A/M*
4 dual phosphorylation, non-bistable	Adapted from 3	neg		dual_phosph_nonbis	K	Kpp
5 High Hill Coefficient	generic	pos		4th_order	M	M4
6 Zero order ultrasensitivity	4	pos		zou_fix	A/M	A/M*
7 Markevich original	3	bis		Markevich	K	Kpp
7b Markevich plus	3,5	bis		Markevich_plus	K	Kpp
7c Markevich plus turnover on KK	3,5	M*bis		Markevich_plus_KK	KK	Not applicable
7d Markevich plus turnover on P	3,5	M*bis		Markevich_plus_P	P	Not applicable
8 MAPK cascade, no fb	6	Pos		acc35_no_fb	MAPK/MAPK	MAPK*
9 MAPK, Huang/Ferrell	7	Pos		acc30	MAPK/MAPK	MAPK/MAPK-PP
10 MAPK entire loop	6	bis followed by neg		acc35	MAPK/MAPK	MAPK*

11 PKC activation	8	Pos/lin		acc48	PKC/PKC-cytosolic	PKC-active
12 Ras/Sos system	9	M*pos		acc1_for_ras	Ras/GDP-Ras	Ras/GTP-Ras
13 Ran traffic, cytoplasmic part	10	Pos/lin		acc70_cyt	Cytoplasm/GDP.Ran-cytoplasmic	Cytoplasm/GTP.Ran-cytoplasmic
14 Ran traffic, nuclear part	10	Pos/lin		acc70_nuc	Nucleus/GDP.Ran-nuclear	Nucleus/GTP.Ran-nuclear
14a Ran traffic both	10	Pos		acc70	Nucleus/GTP.Ran-nuclear	Nucleus/GDP.Ran-nuclear
15 Ras GTPase	11	Pos/lin		acc71_fix	RasGDP	RasGTP
16 Rheb activation	12	Pos/lin		acc87_fix (acc87_Rheb)	Rheb-GDP	Rheb-GTP
17 Gq alone	9	M*Pos		acc16_Gq2	Gq/G-GDP	G*GTP
18 Gq with PLC-beta	9	M*Pos		acc16_Gq	Gq/G-GDP	G*GTP
19 PKA activation	8	M*pos		acc47_PKA	PKA/R2C2	PKA-active
20 TrKB	12	Pos/lin		acc86_fix (acc86_fix_TrKB)	TrKB_mod/TrKB	TrKB_mod/BDNF_TrkB2*_clx
21 PI3K	12	M*Pos		acc86_fix (acc86_fix_PI3K)	PI3K_mod/PI3K	TrKB_mod/Shc*_Grb2-Gab1_Pi3K_clx
22 S6K	12	Neg		acc88	S6Kinase/S6K	S6K_tot
23 AKT activation	12	M*neg		acc87_fix (acc87_AKT)	AKT_mod/AKT	AKT_mod/PIP3_AKT-t308_s473

24 CaMKII CaM-bound form	8	M*neg		acc49 (acc_49_tot_CaM)	CaMKII/CaMKII	CaMKII/tot_CaM_CaMKII
25 CaMKII Autonomous	8	Pos		acc49 (acc_49_tot_auton)	CaMKII/CaMKII	CaMKII/tot_autonomous_CaMKII
26 CaMKII , Ca = 0.2, autonomous	8	Neg		cc49 (acc_49_0.2Ca_auton)	CaMKII/CaMKII	CaMKII/tot_autonomous_CaMKII
27 AMPAR traffic	13	Neg		acc60_PSD5	AMPAR_memb/A_B	AMPAR_memb/A835*845*_B835*845*
28 Rab7	14	Neg		rab7_plus_rab5_fix	A/Rab7.GDP	A/Rab7.GTP
29 Heinrich and Rapoport SNARE	15	M*neg		HR_single_compt_fix	A/M	A/V

Key:

Pos: Positive slope system (for M)

M*Pos: M* exhibits the saturating properties of the positive slope system.

Pos/lin: Both M and M* seem to increase roughly linearly

Neg: Negative slope system for M

M*Neg: Negative slope system for M*

bis: Bistable system where M has the 'breaking wave' shape as Mtot varies.

M*bis: bistable system where M* has the 'breaking wave shape'

Supporting Table S1: Published signaling models fall into 3 categories.

Here I analyzed the characteristic M-vs-Mtot curves for 32 models originating from published papers. The data are arranged in a table with a brief description, literature citation, shape categorization, and plot as the first few columns. The remaining three columns are provided for replicating the analysis, and contain the filename for the model used to generate the curve, the name of the input molecule (M) and the name of the output molecule (M*). The models were taken from DOQCS, the Database of Quantitative Cellular Signaling (<http://doqcs.ncbs.res.in>). They sometimes had to be slightly modified, in case there were buffered forms of the trafficked species, or if some forms had a nonzero initial value that would add onto the supplied Mtot amount. Curves were generated using the MOOSE simulator (<http://moose.ncbs.res.in>) which is backwards-compatible with the GENESIS simulator used for many of the original models in the database. To generate the curves the initial concentration of the trafficked species, M, was assigned starting from 0.01 μM , up to a maximum of 20 μM . The simulation was then integrated numerically and run out for a sufficiently long simulation time to approach steady state. The duration of these runs was estimated manually for each model. Initial concentrations for successive points were incremented logarithmically in factors of 1.1. In each case an adaptive timestep Runge-Kutta-Fehlberg algorithm (GNU Scientific Library) was utilized to carry out ODE calculations to steady-state.

Runs were categorized as bistable, negative-slope and positive slope based on the shape of the resulting M-vs-Mtot curves. Bistable curves were distinguished from negative-slope curves by the presence of a steep drop of M over a single sample point. All the bistable models had already been extensively analyzed in published papers, and this facilitated the classification.

The default nomenclature in these runs was to label the unmodified trafficked molecule as M, and the phosphorylated or otherwise activated molecular state as M*. This did not necessarily give the canonical M-vs-Mtot curves in Figure 3, C(i), E(i) and G(i). In these cases the M* curve usually took the canonical form, and this is indicated in the naming convention as indicated in the Key above.

In a two cases (7c, d) there was no M* state, since these were models of turnover. In these two cases the form of the M curve matched that of the bistable M* curve from Figure 1 C(ii).

In the limit of irreversible reactions it was possible for the bistable regime to have no upper limit as Mtot was increased (e.g. model 7 from Markevich), but this was atypical. The addition of a reversible term to this model restored the regular 'breaking wave' shape of the curve (data not shown).

In a relatively complex bistable model (Model 10, MAPK-PKC feedback loop pathway) involving 81 molecular species and 55 reactions, a negative-slope profile followed the 'breaking wave' shape. Thus the M vs. Mtot response of this complex model combined two of the categories, presumably because of contributions from distinct portions of the model.

References for Supporting Table S1.

1. Ferrell JE, Xiong W (2001) Bistability in cell signaling: How to make continuous processes discontinuous, and reversible processes irreversible. *Chaos* 11, 227-236 .
 2. Ramakrishnan N, Bhalla US (2008) Memory switches in chemical reaction space. *PLoS Comput. Biol* 4, e1000122.
 3. Markevich NI, Hoek JB, Kholodenko BN (2004) Signaling switches and bistability arising from multisite phosphorylation in protein kinase cascades. *J. Cell Biol* 164, 353-359.
 4. Goldbeter A, Koshland DE (1981) An amplified sensitivity arising from covalent modification in biological systems. *Proc. Natl. Acad. Sci. U.S.A* 78, 6840-6844.
 5. Wang X. et al. Bistability, stochasticity, and oscillations in the mitogen-activated protein kinase cascade. *Biophys J* 90, 1961-78(2006).
 6. Bhalla US, Ram PT, Iyengar, R (2002) MAP kinase phosphatase as a locus of flexibility in a mitogen-activated protein kinase signaling network. *Science* 297, 1018-1023.
 7. Huang CY, Ferrell JE (1996) Ultrasensitivity in the mitogen-activated protein kinase cascade. *Proc. Natl. Acad. Sci. U.S.A* 93, 10078-10083.
 8. Bhalla US (2004) Signaling in small subcellular volumes. I. Stochastic and diffusion effects on individual pathways. *Biophys. J* 87, 733-744.
 9. Bhalla US, Iyengar R (1999) Emergent properties of networks of biological signaling pathways. *Science* 283, 381-387.
 10. Görlich D, Seewald MJ, Ribbeck K (2003) Characterization of Ran-driven cargo transport and the RanGTPase system by kinetic measurements and computer simulation. *EMBO J* 22, 1088-1100.
 11. Phillips RA et al. (2003) The mechanism of Ras GTPase activation by neurofibromin. *Biochemistry* 42, 3956-3965.
 12. Jain P, Bhalla US (2009) Signaling logic of activity-triggered dendritic protein synthesis: an mTOR gate but not a feedback switch. *PLoS Comput. Biol* 5, e1000287.
 13. Hayer A, Bhalla US (2005) Molecular switches at the synapse emerge from receptor and kinase traffic. *PLoS Comput. Biol* 1, 137-154.
 14. Del Conte-Zerial P, et al. (2008) Membrane identity and GTPase cascades regulated by toggle and cut-out switches. *Mol. Syst. Biol* 4, 206.
 15. Heinrich R, Rapoport TA (2005) Generation of nonidentical compartments in vesicular transport systems. *J. Cell Biol* 168, 271-280.
-

Supporting Table S2: Literature analyzed for applicability of trafficking motifs.

Citation and title.	Outline	Category
(1) A possible mechanism for self-coordination of bidirectional traffic across nuclear pores	Traffic jams in pore complex leading to two states of movement. Trafficked molecules do not cycle, though the system is bistable.	Bistable but non-cycling
(2) A systems biology approach to analyse amplification in the JAK2-STAT5 signalling pathway	Predicts amplification in Jak-Stat5 shuttling.	Single-state
(3) Identification of nucleocytoplasmic cycling as a remote sensor in cellular signaling by databased modeling	Stat5 shuttling kinetic model using delay-differential equations	Single-state with positive slope.
(4) Dynamics of the Ras/ERK MAPK cascade as monitored by fluorescent probes	MAPK activation and traffic to nucleus, very well parameterized. Many species traffic	Not bistable Too many species to handle.
(5) A mathematical model of the stoichiometric control of Smad complex formation in TGF-beta signal transduction pathway	Model of Smad shuttling. Three species and various other complexes undergo traffic. One set of rates is as fast as the internal reactions	Too many species to handle, possible bistability in switching processes.
(6) Mathematical modeling identifies Smad nucleocytoplasmic shuttling as a dynamic signal-interpreting	Model of Smad shuttling. The system has 5 trafficking species, shows temporal filtering	Not bistable. Too many species to handle.

system		
(7) Oscillatory nucleocytoplasmic shuttling of the general stress response transcriptional activators Msn2 and Msn4 in <i>Saccharomyces cerevisiae</i>	Model of transcriptional activator shuttling. Trafficking steps are faster than reaction steps.	Bistable in nuclear reaction steps, but the trafficking steps are too fast.
(8) Membrane identity and GTPase cascades regulated by toggle and cut-out switches	Model of switching of compartmental state due to Rab5/Rab7.	Bistable, compartmental trafficking amenable to current analysis (see Supporting Figure S1 below).
(9) Oscillations in NF-kappaB signaling control the dynamics of gene expression.	Experiments and models of NF-kappaB oscillations. Multicompartmental.	Oscillatory but trafficking is faster than gene synthesis.
(10) Spontaneous cell polarization through actomyosin-based delivery of the Cdc42 GTPase. (11) A system of counteracting feedback loops regulates Cdc42p activity during spontaneous cell polarization.	Experiments and models of cell polarization through Cdc42 movement.	Positive feedback and state switches, but the movement involves an interplay of Cdc42 and actin. Too many species for current framework.
(12) Simulated de novo assembly of golgi compartments by selective cargo capture during vesicle budding	Simulations of SNARE trafficking	Similar to implemented SNARE model in current paper.

and targeted vesicle fusion		
(13) An Integrated Model of Epidermal Growth Factor Receptor Trafficking and Signal Transduction	Complex multi-compartment model of EGFR signaling and trafficking	Multicompartment model, not bistable.

Supporting Table S2 legend. This table contains brief descriptions and categorization of studies involving trafficking systems that were considered for the current analysis. It does not include the studies used for the dataset of reference models or the studies analyzed in detail in the paper. In summary, there are some 11 studies here that are outside the proposed framework in the current paper. There are a total of 6 studies, between this list and the models implemented in the present paper, that are handled by the current framework. This limited sample suggests that about 35% of trafficking studies fall into the framework established in the current paper.

Supporting Figure S1

Model description for Figure S1.

The conversion of early to late endosomes has been described in a published model of Rab5/7 trafficking by Del Conte-Zerial et al.(8). The trafficking leads to an initial buildup of Rab5, then its abrupt replacement by Rab7. Their original model includes several mutual feedback interactions between Rab5 and Rab7 (Supporting Figure S1 A).

In order to model this in the current framework, I simplified the model and separated out the Rab7 trafficking cycle for analysis. Here the anchor protein P (GDI, guanine nucleotide dissociation inhibitor) binds when the trafficked molecule M (Rab7.GDP) is in the B compartment (Supporting Figure S1 B). The core trafficking reactions (indicated by the dashed outline in Supporting Figure S1 B) can be cast into a trafficking form that is similar to Equation 8, but has the anchor protein binding to molecules in compartment B rather than in A (Supporting Figure S1 C). This gives rise to the following flux-balance equation for the null-cline:

$$MA = (GDF + kb)*(Tot - Atot) / (kf*(Ptot + Atot - Tot))$$

Here

M = Rab

M* = Rab.GTP

P = GDI protein

GDF = GDI displacement factor, acts enzymatically to move M from compartment B to compartment A, simultaneously releasing P.

I implemented the core trafficking ODE models and found that the M-vs-Mtot curve for the compartment A reactions could take the negative-slope or bistable forms depending on parameters. In either case, the trafficking system was bistable for a reasonable range of parameters, as determined by the intersection of null-clines with M-vs-Mtot curves (Supporting Figure S1 D). I also implemented a composite ODE model including the buildup of Rab7 and the replacement of Rab5, to replicate curves from the original study(8) (Supporting Figure S1 E). The original study also included experimental data. Data points were measured from the published figure and overlaid on the simulated curves to show that the model was a good fit to the data (Supporting Figure S1 E).

This model is in supplementary Dataset S1 as rab7_plus_rab5.g.

Figure S1

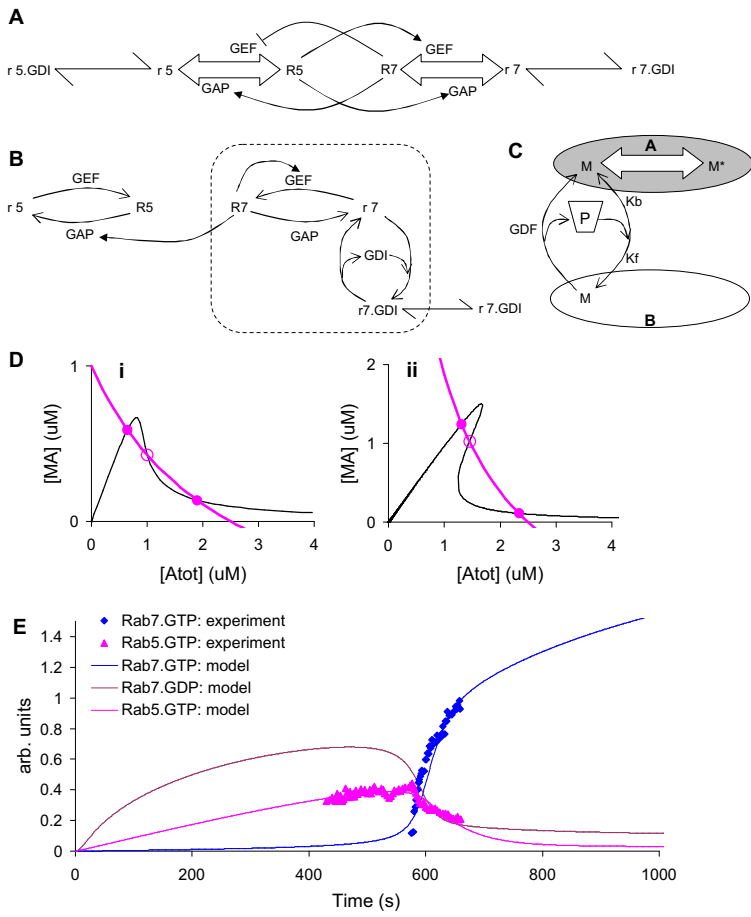


Figure Legend

Supporting Figure S1: Model of compartment state switching and its analysis using the trafficking framework. A. Original complete model reaction scheme. R7 and R5 refer to active forms of Rab 7 and Rab 5 respectively. The inactive forms are r7 and r5. GAP: GTPas activating protein. GEF: Guanine nucleotide exchange factor. GDI: Guanine nucleotide dissociation inhibitor. B. Subset of model examined here. The dashed line outlines the portion to be cast into trafficking form. C. 2-compartmental trafficking representation of Rab 7. GDF is GDI displacement factor. D. Stability analysis for negative-slope (i) and positive-slope (ii) versions of the compartment-A reaction. Both exhibit bistability. E. Full model indicating compartment state switching as the Rab5.GTP form is replaced with Rab7.GTP. Experimental data points are indicated as pink triangles and blue diamonds.

Supporting Text S1: Methods.

Finding and classifying fixed points.

Null clines were obtained by algebraically analyzing the flux-balance conditions, and casting the results in the form of the dependence of M on M_{tot} . Fixed points of the entire trafficked system were determined by finding intersection points between the null cline and the M vs. M_{tot} curve. ODE models were implemented for selected cases using GENESIS/ Kinetikit(14) and loaded into the MOOSE simulator (15) (<http://moose.ncbs.res.in>) which uses the GNU scientific library(16) for linear algebra and numerical integration. Steady-state solutions were obtained by setting the rate equations to zero and using mass-conservation constraints, and solving the resultant system of equations numerically. Stable states were classified by computing the eigenvalues of the Jacobian of the system and inspecting for the sign of the real parts. Additionally, the ODEs were numerically integrated using an adaptive-timestep Runge-Kutta method.

Comparing graphical and steady-state estimates for fixed points

In Figure 4 the graphical (G) and numerical (N) estimates of MA for all the fixed points were compared. I took $\text{abs}(G - N)/(G+N)$ for each fixed point in each panel. In the rare cases where the graphical solution failed to find a fixed point, but the numerical solution did, G was taken as zero. In cases where both values were zero, the difference was taken as zero.

Finding multiple fixed points.

In order to find multiple fixed points for a given model, a MOOSE script function was custom-written for each category of model, to systematically vary the initial conditions of the ODE model while obeying mass-conservation laws. A typical calculation used ~60 such starting points. The script function categorized each distinct solution, to classify the model as a whole. Its main limitation was that it did not always find all the fixed points, especially if there were many closely spaced points. In practice only a small number of the quad-stable cases were affected by this limitation, and these were manually categorized by the graphical analysis.

Generation of state maps.

State maps were generated by scaling two parameters of each of the base trafficking models. The parameters were Total M and ratio of trafficking rates. The stippled state maps were generated where there were multiple parameters, using 2000 Monte Carlo samples of parameters, but plotted only against Total M and ratio of trafficking rates (TR). The solid color maps were computed where there were only the two parameters, by systematic parameter sweeps over each parameter. For each sample in these maps, the parameters of the base model were scaled as follows. The initial concentration of molecule M was set directly to Total M. Trafficking ratios were conceptually the ratio of flux terms into compartment A divided by flux terms out of it. However, care was taken to avoid generating large values of TR lest these invalidate the assumptions of the analysis. For TR greater than one, each of the flux terms into compartment A was divided by TR. For TR less than one, each of the flux terms out of the compartment A was multiplied by TR. The categorization of the model generated in this way was done as described above for finding multiple fixed points, and then counting and classifying each point within the script.

I selected parameter ranges based on physiological estimates for trafficking rates (200 s to 20,000 s), equilibrium constants (0.01 μM to 100 μM), and binding affinities for

anchor protein (0.1 to 10 μM). The interesting molecular concentration ranges were dependent on the region of the M vs M_{tot} curve in which bistable or negative slope effects were present. I chose a range of 1 to 10 μM based on the characteristics of my ODE test models for bistability and negative slope. Systematic and Monte Carlo parameter sweeps for state maps were performed using MOOSE and custom scripts as described above for state classification. Most calculations were done on a cluster (Sun Microsystems, configured by Locuz Systems).

Comparison with models of published trafficking systems

SNARES: I implemented models for SNARE trafficking for positive slope, negative slope, and bistable systems. These were `traff_pp_snare1_BIS`, `traff_nn_snare1_BIS`, and `traff_bb_snare1_BIS` respectively, all of which were bistable. In addition, `traff_bb_snare1_TRI` was tristable. These models are in dataset S1.

CaMKII state switch: The original model for CaMKII was from(17), and is saved as accession 63 in the DOQCS database(18). The M -vs- M_{tot} curves for this model were done using the model `CaMKII_PSD_test.g`, in which the interactions with the AMPAR model, and the trafficking reactions were removed. The predicted 'on' levels of CaMKII were ~ 100 μM (original model ~ 67 μM) and the 'off' level was ~ 2 μM plus a baseline 2 μM (original ~ 8 μM). The level of anchor protein P_{tot} was taken as 720 molecules (120 μM), from the original model. K_{eq} (~ 0.00018) was obtained directly from a dose-response curve on the `CaMKII_PSD_test.g` model, by analyzing responses of the cytosolic pool of CaMKII. The trafficking rates were taken from the original model ($K_{\text{r}} = 0.0333$). T_{ot} was taken as 200 μM , equivalent to the original model level of 1188 molecules.

AMPA traffic: The original model (17), was in accession 60 from DOQCS (`acc60.g`). This was slightly modified to disabling the AMPAR turnover and degradation reactions in order to construct the MA -vs- M_{tot} curve (`acc60_for_turnover.g`). Both models are in Dataset S1.

MAPK oscillator model. This is based on a multisite phosphorylation model(19, 20). These parameters were: $Z = 2 \cdot 10^{-5}$ $\mu\text{M/s}$ and degradation rate = 0.001/s. This was implemented as the ODE model `Markevich_KK_OSC.g`.

All these models are included in the collection of models in Dataset S1.

References

1. Kapon, R., A. Topchik, D. Mukamel, and Z. Reich. 2008. A possible mechanism for self-coordination of bidirectional traffic across nuclear pores. *Phys Biol.* 5: 036001.
2. Vera, J., J. Bachmann, A.C. Pfeifer, V. Becker, J.A. Hormiga, et al. 2008. A systems biology approach to analyse amplification in the JAK2-STAT5 signalling pathway. *BMC Syst Biol.* 2: 38.
3. Swameye, I., T.G. Muller, J. Timmer, O. Sandra, and U. Klingmuller. 2003. Identification of nucleocytoplasmic cycling as a remote sensor in cellular signaling by databased modeling. *Proc. Natl. Acad. Sci. U.S.A.* 100: 1028-1033.
4. Fujioka, A., K. Terai, R.E. Itoh, K. Aoki, T. Nakamura, et al. 2006. Dynamics of the Ras/ERK MAPK cascade as monitored by fluorescent probes. *J. Biol. Chem.* 281: 8917-8926.
5. Nakabayashi, J., and A. Sasaki. 2009. A mathematical model of the stoichiometric control of Smad complex formation in TGF-beta signal transduction pathway. *J. Theor. Biol.* 259: 389-403.
6. Schmierer, B., A.L. Tournier, P.A. Bates, and C.S. Hill. 2008. Mathematical modeling identifies Smad nucleocytoplasmic shuttling as a dynamic signal-interpreting system. *Proc. Natl. Acad. Sci. U.S.A.* 105: 6608-6613.
7. Jacquet, M., G. Renault, S. Lallet, J. De Mey, and A. Goldbeter. 2003. Oscillatory nucleocytoplasmic shuttling of the general stress response transcriptional activators Msn2 and Msn4 in *Saccharomyces cerevisiae*. *J. Cell Biol.* 161: 497-505.
8. Del Conte-Zerial, P., L. Bruschi, J.C. Rink, C. Collinet, Y. Kalaidzidis, et al. 2008. Membrane identity and GTPase cascades regulated by toggle and cut-out switches. *Mol. Syst. Biol.* 4: 1-9.
9. Nelson, D.E., A.E.C. Ihekweaba, M. Elliott, J.R. Johnson, C.A. Gibney, et al. 2004. Oscillations in NF-kappaB signaling control the dynamics of gene expression. *Science.* 306: 704-8.
10. Wedlich-Soldner, R., S. Altschuler, L. Wu, and R. Li. 2003. Spontaneous cell polarization through actomyosin-based delivery of the Cdc42 GTPase. *Science.* 299: 1231-1235.
11. Ozbudak, E.M., A. Becskei, and A. van Oudenaarden. 2005. A system of counteracting feedback loops regulates Cdc42p activity during spontaneous cell polarization. *Dev. Cell.* 9: 565-571.

12. Gong, H., D. Sengupta, A.D. Linstedt, and R. Schwartz. 2008. Simulated de novo assembly of golgi compartments by selective cargo capture during vesicle budding and targeted vesicle fusion. *Biophys. J.* 95: 1674-1688.
13. Resat, H., J.A. Ewald, D.A. Dixon, and H.S. Wiley. 2003. An Integrated Model of Epidermal Growth Factor Receptor Trafficking and Signal Transduction. *Biophysical Journal.* 85: 730-743.
14. Bhalla, U.S. 2002. Use of Kinetikit and GENESIS for modeling signaling pathways. *Meth. Enzymol.* 345: 3-23.
15. Ray, S., and U.S. Bhalla. 2008. PyMOOSE: Interoperable Scripting in Python for MOOSE. *Front Neuroinformatics.* 2: 6.
16. Galassi, M., J. Davies, B. Theiler, G. Gough, P. Jungman, et al. 2009. GNU Scientific Library Reference Manual. 3rd ed. Bristol: Network Theory.
17. Hayer, A., and U.S. Bhalla. 2005. Molecular switches at the synapse emerge from receptor and kinase traffic. *PLoS Comput. Biol.* 1: 137-154.
18. Sivakumaran, S., S. Hariharaputran, J. Mishra, and U.S. Bhalla. 2003. The Database of Quantitative Cellular Signaling: management and analysis of chemical kinetic models of signaling networks. *Bioinformatics.* 19: 408-415.
19. Wang, X., N. Hao, H.G. Dohlman, and T.C. Elston. 2006. Bistability, stochasticity, and oscillations in the mitogen-activated protein kinase cascade. *Biophys J.* 90: 1961-78.
20. Markevich, N.I., J.B. Hoek, and B.N. Kholodenko. 2004. Signaling switches and bistability arising from multisite phosphorylation in protein kinase cascades. *J. Cell Biol.* 164: 353-359.